

Physically-Consistent Generative Adversarial Networks for Coastal Flood Visualization

Björn Lütjens*, Brandon Leshchinskiy*, Christian Requena-Mesa*, Farrukh Chishtie*, Natalia Díaz-Rodríguez*, Océane Boulais*, Aruna Sankaranarayanan*, Margaux Masson-Forsythe*, Aaron Piña, Yarin Gal, Chedy Raïssi, Alexander Lavin, Dava Newman

As climate change increases the intensity of natural disasters, society needs better tools for adaptation. Floods, for example, are the most frequent natural disaster, and better tools for flood risk communication could increase the support for flood-resilient infrastructure development. Our work aims to enable more visual communication of large-scale climate impacts via visualizing the output of coastal flood models as satellite imagery. We propose the first deep learning pipeline to ensure physical-consistency in synthetic visual satellite imagery. We advanced a state-of-the-art GAN called *pix2pixHD*, such that it produces imagery that is physically-consistent with the output of an expert-validated storm surge model (NOAA SLOSH). By evaluating the imagery relative to physics-based flood maps, we find that our proposed framework outperforms baseline models in both physical-consistency and photorealism. We envision our work to be the first step towards a global visualization of how the climate challenge will shape our landscape. Continuing on this path, we show that the proposed pipeline generalizes to visualize reforestation. We also publish a dataset of over 25k labelled image-triplets to study image-to-image translation in Earth observation¹.

Index Terms—Physics-Informed Neural Networks, Generative Adversarial Networks, Synthetic Data Generation, Deep Generative Vision Models, Climate Change, Flood Inundation Models, Visualization.

*indicates equal contribution. Corresponding author: B. Lütjens; lutjens@mit.edu.

BLü, BLE, and DN are with the Massachusetts Institute of Technology, CRM with the Max Planck Institute for Biogeochemistry. FC with the Spatial Informatics Group. NDR with the Institut Polytechnique Paris. OB with the MIT Media Lab. MMF with Earthshot Labs. AS with the MIT Media Lab. AP with the National Aeronautics and Space Administration (NASA) Headquarters. YG with Oxford University. CR with Ubisoft. AL with Latent Sciences.

BLü is leading the work. BLE started the work. All authors contributed to study design. BLü, BLE, CRM, FC, NDR, OB, and AL contributed equally to flood data processing, model implementation, and evaluation. AS contributed the ice experiment. MMF contributed to reforestation experiment. BLü contributed the other generalization experiments. AP contributed expertise in flooding and stakeholder engagement, YG and CR in deep learning, and DN in human-computer interfaces.

¹Code and data will be open-sourced at github.com/frontierdevelopmentlab/fdl-us-2020-earth-engine upon publication; an interactive demo is available at climate-viz.github.io.



Fig. 1: The *Earth Intelligence Engine* generates physically-consistent satellite imagery of future coastal flood events to aid in climate communication. Explore more results in high-resolution at climate-viz.github.io.

I. INTRODUCTION

Our climate changes, causing natural disasters to become more intense [1]. Floods are the most frequent weather-related disaster [2] and already cost the U.S. 3.7B USD per year [3]; this damage is projected to grow over the next decades [1]. Visualizations of climate impacts are widely used by policy and decision makers to raise environmental awareness and facilitate dialogue on long-term climate adaptation decisions [4]. Current visualizations of coastal flood impacts, however, are limited to color-coded flood maps [5] or synthetic street-view imagery [6], which do not convey city-wide flood impacts in a compelling manner, as shown in Fig. 2 and [7]. Our work generates synthetic satellite imagery of future coastal floods, informed by the projections of expert-validated flood models, to enable a more engaging communication of city-wide flood risks to governmental offices.

Generative adversarial networks (GANs) have been used to generate highly photorealistic imagery of faces [12], [13], animals [14], [15], or even street-level flood imagery [10]. Recent works, have adapted GANs to generate satellite imagery [16], [17], [18], [19], [20]. Synthetic satellite imagery, however, needs to be trustworthy [21]. While many approaches exist to increase the trustworthiness of neural network-based models, including interpretable networks [22], adversarial robustness [23], [24], or ensemble predictions [25], [26], this work focuses on ensuring physical-consistency.

Many recent works incorporate domain knowledge from the physical sciences into deep learning [27], [28], [29], [30]. Our

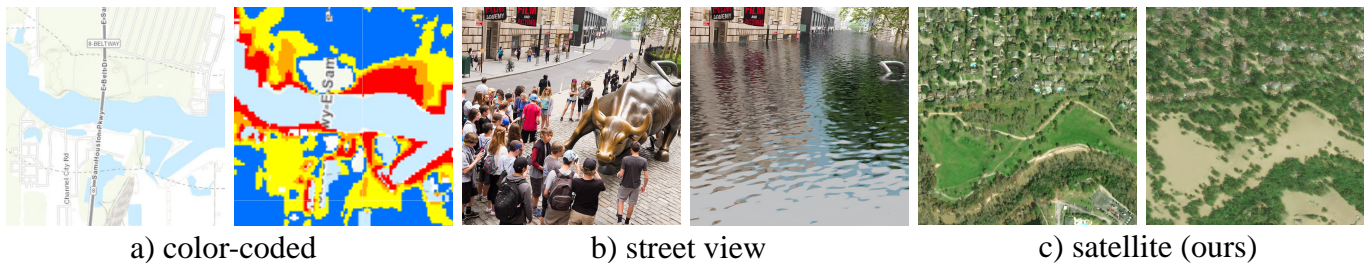


Fig. 2: **Physically-consistent satellite imagery (c) could enable more engaging and reliable communication of city-scale flood risks** [4]. Most existing visualizations of coastal floods or sea-level rise that are aimed towards the public rely on color-coded geospatial rasters (a), that can be unrelatable or impersonal [5], [8], [9]. Alternative photorealistic visualizations are often limited to local street-level imagery (b) [6], [10] that lack further spatial context. Image sources: [5], [5], [6], [6], [11], ours.

work aims to generate physically-consistent imagery, whereas we define an image as physically-consistent if it depicts the same flood extent as an expert-validated coastal flood model, as detailed in Section III-C. To achieve physical-consistency, one could adapt the neural network architecture to incorporate physics as: inputs [31], training loss [32], the learned representation [33], [34], [22], hard output constraints [35], or evaluation function [36]. Alternatively, one could embed the neural network in differential equations [37], for example, as: parameters [38], [32], dynamics [39], residual [40], [41], differential operator [27], [42], or solution [32]. Our work is the first in leveraging any of these methods to ensure physical-consistency in synthetic visual satellite imagery, to the extent of the authors’ knowledge. Specifically, our work leverages years of scientific domain knowledge by incorporating physics-based coastal flood model projections as neural network input and evaluation function. Exploring the alternative forms of physical consistency for satellite imagery is an exciting field left for future works.

Our work makes five contributions:

- the first generative vision pipeline to synthesize physically-consistent visual satellite imagery, called the *Earth Intelligence Engine*,
- the first physically-consistent and photorealistic visualization of flood risks as satellite imagery,
- a novel metric, the Flood Visualization Plausibility Score (FVPS), to evaluate the photorealism and physical-consistency of generated imagery,
- the first visualization of future reforestation as satellite imagery, and
- an open-source dataset with over 25k labelled high-resolution image-triplets to study image-to-image translation in Earth observation.

II. RELATED WORK

Our work combines a coastal flood model with a generative vision model in a novel physically-consistent pipeline to create visualizations of coastal floods.

A. Generative vision modeling.

We aim to learn the change in satellite imagery from before to after a coastal flood, which is similar to paired image-

to-image translation [12]. Within image-to-image translation models, generative adversarial networks (GANs) generated samples of highly photorealistic imagery. For example, semantic image synthesis models generated photorealistic street scenery from semantic segmentation masks: DCGAN [43], Pix2pixHD [13], DRPAN [44], SPADE [45], or OASIS [46]. In comparison to GANs, normalizing flows [47], [26] or variational autoencoders [48] capture the distribution of possible image-to-image translations more accurately [49], but single samples often look less realistic ([50], [51], Fig. 4). Because our use case requires photorealism we focus on GANs and extend the high-resolution semantic image synthesis model, pix2pixHD [13], to take in physical information and produce imagery that is both photorealistic and physically-consistent. We leave ensemble predictions capturing the full distribution of images for future work.

B. Physics-informed deep learning.

Physics-informed deep learning has recently generated significant excitement. It promises to increase trust, interpretability, and data-efficiency of deep learning models [27], [28], [31]. The *Earth Intelligence Engine* incorporates a physics-based coastal flood model as input and evaluation function and is the first in the physics-informed deep learning literature to generate physically-consistent satellite imagery [31]. Future works will extend the connections between physics and deep learning-generated satellite imagery. For example, [52] could be used to learn a physically-interpretable latent space, e.g., a “flood neuron“, [53] to embed deep learning in atmospheric noise models, or [46] to incorporate physics-based flood maps in the loss function.

C. Climate change visualization tools

Visualizations of climate change are commonly used in policy making and community discussions on climate adaptation [4], [54]. Landscape visualizations are used to raise environmental awareness in the general public or policy [7], [10], because they can convey the impacts of climate change, such as rising sea levels or coastal floods, in a compelling and engaging manner ([7], Fig. 2b). Most landscape visualizations, however, are limited to regional information [6]. Additionally,

most landscape visualizations require expensive physics-based renderings and/or high-resolution digital elevation models [6]. Alternative visualization tools of coastal floods or sea-level rise are color-coded maps, such as [55], [5], [9]. Color-coded maps convey the flood extent on a city-wide scale, but are less engaging than a photorealistic image [4]. We are generating compelling visualizations of future coastal floods as satellite imagery to aid in policy and community discussion on climate adaptation.

III. APPROACH

The proposed pipeline uses a generative vision model to generate post-flood images from pre-flood images and a flood extent map, as shown in Fig. 3.

A. Data Overview.

Obtaining ground-truth post-flood images that display standing water is challenging due to cloud-cover, time of standing flood, satellite revisit rate, increased atmospheric noise, and cost of high-resolution imagery. This work leverages the xBD dataset [11], a collection of pre- and post-disaster images from events like Hurricane Harvey or Florence, from which we obtained ~ 3 k pre- and post-flood image pairs with the following characteristics: $\sim .5$ m/px, RGB, 1024×1024 px/img, Maxar DigitalGlobe.

The coastal flood model is the *Sea, Lake and Overland Surges from Hurricanes* (SLOSH) model [56], developed by the National Weather Service (NWS). SLOSH estimates storm surge heights from atmospheric pressure, hurricane size, forward speed, and track data, which are used as a wind model driving the storm surge. The SLOSH model consists of shallow water equations, which consider unique geographic locations, features, and geometries. The model is run in deterministic, probabilistic, and composite modes by various agencies for different purposes, including NOAA, National Hurricane Center (NHC) and NWS. We use outputs from the composite approach – that is, running the model several thousand times with hypothetical hurricanes under different storm conditions. As a result, we obtain a binary flood hazard map from [5] as displayed in Fig. 2a which are storm-surge, height-differentiated, flood extents at 30 m/px resolution. The flood hazard maps do not intersect with the locations of existing post-flood imagery. To get around the data limitation, we generate and coarse-grain segmentation maps of the post-flood imagery to 30 m/px for training and evaluation and use binarized flood hazard maps during test. Future works will extend the state-of-the-art *ADvanced CIRCulation* model (ADCIRC) [57] model, which is described in [8] and has a stronger physical foundation with better accuracy, and higher resolution than SLOSH.

B. Model architecture.

The central model of our pipeline is a generative vision model that learns the physically-conditioned image-to-image transformation from pre-flood image to post-flood image. We leveraged the existing implementation of pix2pixHD [13].

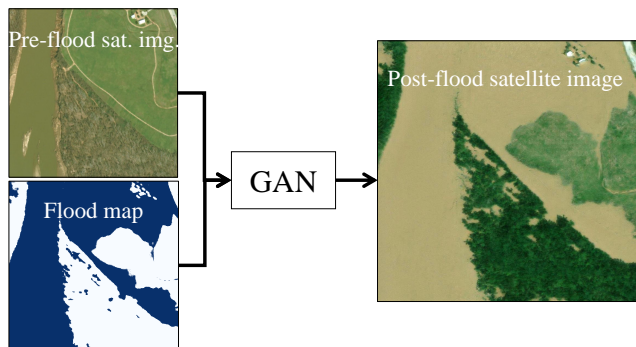


Fig. 3: Model Architecture. Our model leverages the semantic image synthesis model, Pix2pixHD [58], and combines a pre-flood satellite image with a physics-based flood map to generate post-flood satellite imagery.

Pix2pixHD is a state-of-the-art semantic image synthesis model that uses multi-scale generator and discriminator architectures to generate high-resolution imagery. We extended the input dimensions to $1024 \times 1024 \times 4$ to incorporate the flood extent map and found in extensive hyperparameter experiments that the default parameters in [58] work best. The resulting pipeline is modular, such that it can be repurposed for visualizing other climate impacts.

C. Physically-consistent image.

We define a *physically-consistent* model as one that fulfills laws of physics, such as, conservation of momentum, mass, and energy [28]. For example, most coastal flood models consist of numerical solvers that resolve the conservation equations to generate flood extent predictions [56]. Here, we consider an image to be physically-consistent if it depicts the predictions of a physically-consistent model.

Specifically, we define our generated satellite imagery, $I_G \in \mathcal{I} = [0, 1]^{w \times h \times c}$ with width, $w = 1024$, height, $h = 1024$, and number of channels, $c = 3$, to be physically-consistent if it depicts the same flood extent as the binary flood map, $F \in \mathcal{F} = \{0, 1\}^{w \times h}$. We implemented a flood segmentation model, $m_{\text{seg}} : \mathcal{I} \rightarrow \mathcal{F}$, to measure the depicted flood extent in the generated image. If the flood extent of a generated image and the coastal flood model match within a margin, the image is in the set of physically-consistent images, i.e., $\mathcal{I}_{\text{phys}} = \{I_G \in \mathcal{I} : \|m_{\text{seg}}(I_G) - F\| < \epsilon\}$. The generated image is considered photorealistic, if it is contained in the manifold of naturally possible satellite images, $\mathcal{I}_{\text{photo}} \subset \mathcal{I}$. Hence, we are looking for a conditional image generation function, g , that generates an image that is both, physically-consistent and photorealistic, i.e., $g : \mathcal{I}_{\text{photo}} \times \mathcal{F} \rightarrow \mathcal{I}_{\text{photo}} \cap \mathcal{I}_{\text{phys}}$. Here, we condition the GAN on the flood map, F , and use a custom evaluation function to identify the generation function, g .

D. The Evaluation Metric Flood Visualization Plausibility Score (FVPS).

Evaluating imagery generated by a GAN is difficult [59], [60]. Most evaluation metrics measure photorealism or sample

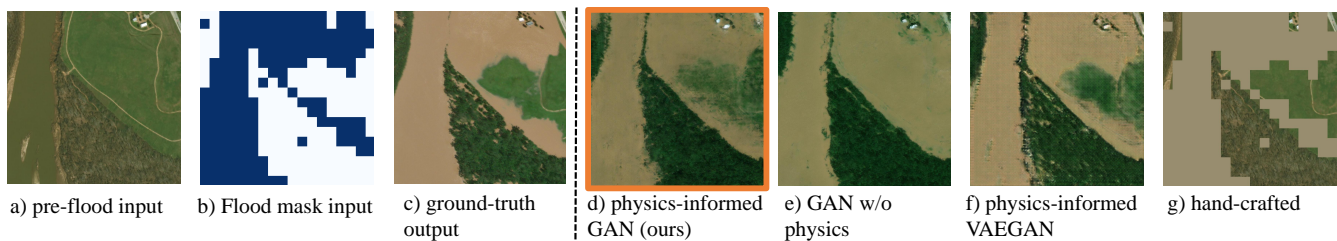


Fig. 4: **The proposed physics-informed GAN, (d), generates photorealistic and physically-consistent flood imagery from the inputs, (a,b), outperforming all other models, (e,f,g).** The baseline GAN, pix2pixHD [13] (e), in comparison, receives only a pre-flood image and no physical input. The resulting image, (e), is fully-flooded, rendering the model untrustworthy. The VAEGAN, BicycleGAN [51] (f), creates glitchy imagery (zoom in). A handcrafted baseline model (g), as used in common visualization tools [9], [55], visualizes the correct flood extent, but is pixelated and lacks photorealism.

diversity [60], but not physical consistency [61] (see, e.g., SSIM [62], MMD [63], IS [64], MS [65], FID [66], [67], or LPIPS [68]).

To evaluate physical consistency we propose using the intersection over union (IoU) between water in the generated imagery and water in the flood extent map. This method relies on flood masks, but because there are no publicly available flood segmentation models for Maxar RGB satellite imagery, we trained our own model on ~ 100 hand-labeled flooding images (Section IV-B). This segmentation model produced flood masks of the generated and ground-truth flood image which allowed us to measure the overlap of water in between both. When the flood masks overlap perfectly, the IoU is 1; when they are completely disjoint, the IoU is 0.

To evaluate photorealism, we used the state-of-the-art perceptual similarity metric Learned Perceptual Image Patch Similarity (LPIPS) [68]. LPIPS computes the feature vectors (of an ImageNet-pretrained AlexNet CNN architecture) of the generated and ground-truth tile and returns the mean-squared error between the feature vectors (best LPIPS is 0, worst is 1).

Because the joint optimization over two metrics poses a challenging hyperparameter optimization problem, we propose to combine the evaluation of physical consistency (IoU) and photorealism (LPIPS) in a new metric (FVPS), called Flood Visualization Plausibility Score (FVPS). The FVPS is the harmonic mean over the submetrics, IoU and $(1 - \text{LPIPS})$, that are both $[0, 1]$ -bounded. Due to the properties of the harmonic mean, the FVPS is 0 if any of the submetrics is 0; the best FVPS is 1. In other words, the FVPS is only 1 if the imagery is both photorealistic and physically-consistent.

$$\text{FVPS} = \frac{2}{\frac{1}{\text{IoU} + \epsilon} + \frac{1}{1 - \text{LPIPS} + \epsilon}}. \quad (1)$$

IV. EXPERIMENTAL RESULTS

A. Physical-consistency and photorealism.

In terms of both physical-consistency and photorealism, our physics-informed GAN outperforms an unconditioned GAN that does not use physics, as well as a handcrafted baseline model (Fig. 4).

1) *A GAN without physics information generates photorealistic but non physically-consistent imagery.*

The inaccurately modeled flood extent in Fig. 4e illustrates the physical-inconsistency and a low IoU of 0.226 in Table I over the test set further confirms it (see Section A for test set details). Despite the photorealism (LPIPS = 0.293), the physical-inconsistency renders the model non-trustworthy for critical decision making, as confirmed by the low FVPS of 0.275. The model is the default pix2pixHD [13], which only uses the pre-flood image and no flood mask as input.

2) *A handcrafted baseline model generates physically-consistent but not photorealistic imagery.*

Similar to common flood visualization tools [9], the handcrafted model overlays the flood mask input as a hand-picked flood brown (#998d6f) onto the pre-flood image, as shown in Fig. 4g. Because typical storm surge models output flood masks at low resolution ($30m/px$ [5]), the handcrafted baseline generates pixelated, non-photorealistic imagery. Combining the high IoU of 0.361 and the poor LPIPS of 0.415, yields a low FVPS score of 0.359, highlighting the difference to the physics-informed GAN in a single metric.

3) *The proposed physics-informed GAN generates physically-consistent and photorealistic imagery.*

To create the physics-informed GAN, we trained pix2pixHD [13] from scratch on our dataset (200 epochs in ~ 7 hrs on $8 \times V100$ Google Cloud GPUs). This model successfully learned how to convert a pre-flood image and a flood mask into a photorealistic post-flood image, as shown in Fig. 1. The model outperformed all other models in IoU (0.553), LPIPS (0.263), and FVPS (0.532) (Table I). The learned image transformation “in-paints” the flood mask in the correct flood colors and displays an average flood height that does not cover structures (e.g., buildings, trees), as shown in 64 randomly sampled test images in Fig. 5. Occasionally, city-scenes show scratch patterns, e.g., Fig. 5 (top-left). This could be explained by the unmodeled variance in off-nadir angle, sun inclination, GPS calibration, color calibration, atmospheric noise, dynamic objects (cars), or flood impacts, which is partially addressed in Section IV-C1. While our model also outperforms the VAEGAN (BicycleGAN), the latter has the potential to create ensemble forecasts over the unmodeled flood impacts, such as the probability of destroyed buildings.



Fig. 5: **Generated post-flooding imagery of 64 randomly chosen tiles** of hurricanes Harvey and Florence test set.

B. Flood segmentation model.

The flood segmentation model was a pix2pix segmentation model [12], which uses a vanilla U-net as generator. The model was trained from scratch to minimize $L1$ -loss, IoU, and adversarial loss and had the last layers finetuned on $L1$ -loss. We hand-labelled pixel-wise flood maps of 111 post-flood images to train the model. A four-fold cross validation was performed leaving 23 images for testing. The segmentation model selected to be used by the FVPS has a mean IoU performance of 0.343. Labelled imagery will be made available as part of the dataset.

C. Generalization performance.

So far, we showed that our pipeline can generate post-flood imagery at select locations, such as hurricane Harvey in Houston, TX, and for matching remote sensing instruments between train and test, e.g., Maxar satellite. The *Earth Intelligence Engine*, however, aims to visualize global impacts of the climate challenge as seen from space. This section evaluates the generalization capability across location, remote sensing instrument, and climate phenomena.

1) Generalization across location and remote sensing instruments.

To visualize coastal flooding across the U.S. East coast our model needs to generalize across location and remote sensing instrument. We trained our model with pre-flood image tiles from Maxar. Maxar imagery across the U.S. East Coast, however, is not freely available. Hence, we assembled a dataset of pre-flood image tiles from the open-access U.S.-wide mosaic of $1.0m/px$ visual aerial imagery from the 2019 National Agriculture Imagery Program (NAIP) [69]. The pre-flood NAIP image tiles are paired with open-access Maxar post-flood satellite imagery and a generated pixelwise flood segmentation mask. This creates a dataset of 6500 clean image-triplets that we are releasing as the flood-section of our open-source dataset to study image-to-image (im2im) translation in Earth observation.

The im2im translation task from NAIP aerial to Maxar satellite imagery is significantly more challenging than the Maxar→Maxar task, because the learned image-transformation needs to account for differing remote sensing

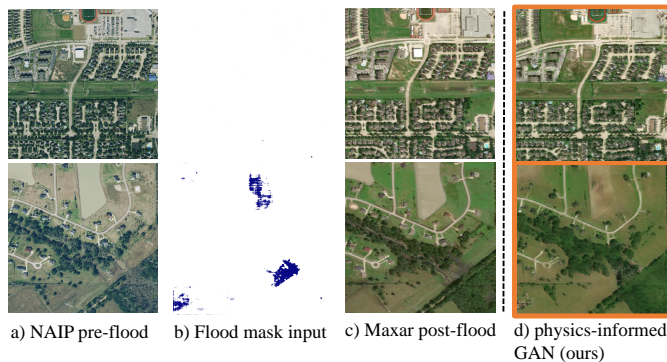


Fig. 6: **Generalization across remote sensing instruments.** We have compiled a dataset of 6500 image-pairs to generalize across remote sensing instruments, here predicting $0.5m/px$ Maxar satellite imagery (output) from $1.0m/px$ aerial NAIP imagery. While the generated imagery (right) is not production ready it suggests that the model can learn across different remote sensing instruments, learning the change in resolution, flight altitude, color calibration, and atmospheric noise magnitude.

instruments, flight altitude, atmospheric noise magnitude, color calibration, and more. To reduce the learning task complexity, we removed the variation within Maxar data, via sourcing post-flood tiles from a single satellite pass over west Houston, TX on 8/31/2017, post-hurricane Harvey [70]. To re-run our pipeline, we labelled 260 flood segmentation masks (in ~ 2 hrs), retrained the flood segmentation model, and retrained the physics-informed GAN from scratch on the new dataset (for 15 epochs in ~ 5 hrs on $1 \times V100$ GPU). The resulting model did not outperform the baseline in physical-consistency, which is likely due to the suboptimal performance of this dataset’s segmentation model (IoU=0.23). However, the resulting model still outperforms the baseline in photorealism (LPIPS=0.369 vs. 0.465) on a 20% test split. While these flood maps are not ready for production our research shows that im2im translation across remote sensing instruments is feasible, as well as, the potential to visualize coastal flooding along the full U.S. East Coast.

2) Generalization across climate phenomena – visualizing reforestation

Visualizing negative climate impacts can evoke anger, fear, or guilt which can encourage pro-environmental behavior [71], [72], [73], respectively. These emotions can, however, also feel overwhelming [74] and hope is needed to maintain environmental engagement [75]. Here we extend the *Earth Intelligence Engine* to visualize the impact of positive action, specifically, to encourage policymakers, investors, and landowners to reforestation.

To synthesize satellite imagery of reforested land, the *Earth Intelligence Engine* uses an image of a deforested area along with a binary mask of where trees will be planted as input. To train and evaluate the model we collected image-triplets of an RGB pre-reforestation image, a binary reforestation area mask (1=reforestation), and an RGB post-reforestation image,

	LPIPS high res.	LPIPS low res.	IoU high res.	IoU low res.	FVPS high res.	FVPS low res.
GAN w/ phys. (ours)	0.265	0.283	0.502	0.365	0.533	0.408
GAN w/o phys.	0.293	0.293	0.226	0.226	0.275	0.275
VAEGAN w/ phys.	0.449	-	0.468	-	0.437	-
Handcrafted baseline	0.399	0.415	0.470	0.361	0.411	0.359

TABLE I: **In terms of photorealism (LPIPS) and physical consistency (IoU), our physics-informed GAN outperforms three benchmarks:** the baseline GAN without physics; a physics-informed VAEGAN; and a handcrafted baseline. The proposed Flood Visualization Plausibility Score (FVPS) trades-off IoU and LPIPS as a harmonic mean and highlights the performance differences between the GAN with and without physics on low-resolution flood mask inputs.

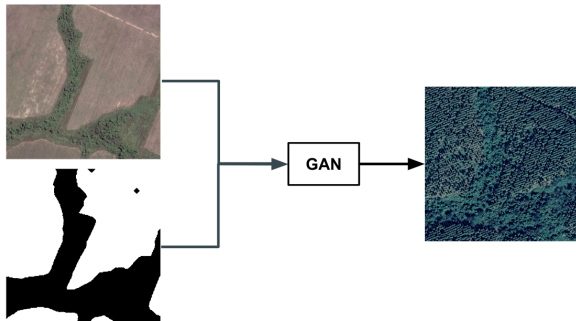


Fig. 7: **Model Architecture for Reforestation.** Our model leverages the semantic image synthesis model, Pix2pixHD [58], and combines a pre-forestation satellite image with a reforestation map to generate post-forestation satellite imagery.

as illustrated in Fig. 7. We assembled a total of 1026 train and 246 test high-resolution (50cm/px) 1024x1024 image-triplets via Google Earth Pro (Map data: Google, Maxar Technologies, CNS/Airbus). The dataset spans four different countries: Uruguay, Sierra Leone, Peru, and Mexico, as detailed in Section A.

We trained the generative vision model that performed best on floods, pix2pixHD, using several augmentation techniques and the default [13] hyperparameters, as detailed in Section B-A. We evaluated the model on a random split and a spatial, i.e., test on held-out 107 images from Guatemala, split using LPIPS loss and compare it to a baseline model that applies uniformly colored masks.

Figure 8d) shows how our model generates photorealistic visualizations of reforestation projects. The generated imagery looks more realistic than handcrafted baseline models (e,f), where the reforested area pixels are set to a mean forest color. Our quantitative analysis in Table II confirms that our model outperforms the baselines in both random and spatial split. Note however that LPIPS has limits as distance metric, because the ground-truth post-forestation image often contained unknown features such as newly built houses.

3) Visualizing Arctic sea ice melt

The retreat of Arctic sea ice is one of the most important and imminent consequences of climate change [1]. However, visualizations of melting Arctic sea ice are limited to physics-based renderings, such as [76]. There also does not exist

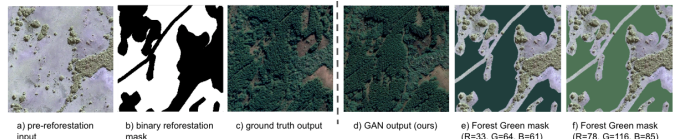


Fig. 8: **Reforestation.** The proposed pix2pixHD [13] GAN, (d), generates photorealistic and consistent reforestation imagery from the inputs, (a,b), outperforming baseline models (e,f).

daily high-resolution ($\approx 500\text{m}$) visual satellite imagery due to satellite revisit rate and cloud cover. To enable the extension of the *Earth Intelligence Engine* for visualizing Arctic sea ice melt, we publish a dataset of $\approx 20k$ image pairs of Winter image, Summer image, and ice segmentation mask, as detailed in Section A.

V. DISCUSSION AND FUTURE WORK

1) Limitations.

Although our pipeline outperformed all baselines in the generation of physically-consistent and photorealistic imagery of coastal floods, there are areas for improvement in future works. For example, our flood datasets only contained $3k$ or $6.5k$ samples and were biased towards vegetation-filled satellite imagery; this data limitation likely contributes to our model rendering human-built structures, such as streets and out-of-distribution skyscrapers in Fig. 5 top-left, as smeared. Although we attempted to overcome our data limitations by using several state-of-the-art augmentation techniques (see Section B), this work would benefit from more public sources of high-resolution satellite imagery and large foundation models that are pretrained on remote sensing data [77]. Apart from the data limitation, smeared features are still a current concern in state-of-the-art GAN architectures [46]. Furthermore, the computational intensity of training GANs made it difficult to optimize the models on new data. Improved transfer learning techniques could address this challenge. Lastly, satellite imagery is an internationally trusted source for analyses in deforestation, development, or military domains [78], [79]. With the increased capability of data-generating models, more work is needed in the identification of and the education around misinformation and ethical and trustworthy AI [21]. We point out that our satellite imagery is synthetic, should only be used as communication aid [4], and we take first steps towards guaranteeing trustworthiness in synthetic satellite imagery.

	LPIPS random split	LPIPS spatial split
GAN (ours)	0.5033	0.5735
Green mask (RGB=33,64,61)	0.7942	0.8478
Green mask (RGB=78,116,85)	0.8453	0.9567

TABLE II: **Our model quantitatively outperforms two baseline models that apply a color mask in a random and spatial split.**

2) Cloud-penetrating satellite imagery.

Remote sensing commonly faces the problem of missing frames, due to cloud-cover, orbital alignment, or cost of high-resolution imagery [80], [81]. The *Earth Intelligence Engine* can be seen as a gap-filling model that combines the information from low-resolution flood maps and high-resolution pre-flood image mosaics to infer the missing high-resolution post-flood satellite imagery. For example after floods, the arrival of the first visual images is often delayed until clouds pass or expensive drone surveys are conducted. Synthetic-aperture radar (SAR) is cloud-penetrating and often returns the first available medium-resolution flood maps (at ~ 10 m/px) [82]. The *Earth Intelligence Engine* could visualize the medium-resolution SAR-derived flood extent maps. However, future work will be necessary to extend the trustworthiness of generated flood visualizations in disaster response, for example, via incorporating information on the flood height, building damage, or the raw SAR signal. The current visualizations are aimed towards media or policy to communicate the possible extent of future floods in a compelling manner [4].

3) Vision for the future.

We envision a global visualization tool of climate impacts and adaptation techniques. By changing the input data, future work can visualize impacts of other well-modeled, climate-attributed events, including Arctic sea ice melt, hurricanes, wildfires, or droughts. Non-binary climate impacts, such as inundation height, or drought strength could be generated by replacing the binary flood mask with continuous model predictions. Opportunities are abundant for further work in visualizing our changing Earth. This work opens exciting possibilities in generating physically-consistent imagery with potential impact on improving climate mitigation and adaptation.

March 12, 2021

VI. ACKNOWLEDGEMENTS

This research was conducted at the Frontier Development Lab (FDL), US. The authors gratefully acknowledge support from the MIT Portugal Program, National Aeronautics and Space Administration (NASA), and Google Cloud.

We are very thankful for Margaret Maynard-Reid and Leo Silverberg for generating the demo at trillium.tech/eie. We thank Ritwik Gupta for the continuous help in using the xBD dataset, Richard Strange for the help with cloud compute, Prof. Marco Tedesco for advise on the Arctic sea ice, Guy Schumann on flood modeling, Mark Veillette and Cait Crawford for technical direction, and James Parr, Leah Lovgren, Sara Jennings and Jodie Hughes for the organization of FDL and enabling these connections. We greatly appreciate the advise on

decision-/policymaking in coastal climate adaptation by Derek Loftis, Sagy Cohen, Capt. John Radovan, Maya Nasr, and Janot Mendler de Suarez. Further, we greatly appreciate the technical feedback and direction from Esther Wolff, Hannah Munguia-Flores, Peter Morales, Nicholas Mehrle, Prof. Bistra Dilkina, Freddie Kalaitzis, Graham Mackintosh, Michael van Pohle, Gail M. Skofronick-Jackson, Tsengdar Lee, Madhulika Guhathakurta, Julien Cornebise, Maria Molina, Massy Mascaro, Scott Penberthy, John Karcz, Jack Kaye, Campbell Watson, and all other FDL researchers.

The authors also gratefully acknowledge support from Earthshot Labs for their work on the reforestation visualization. Further, we greatly appreciate the time, feedback, direction, and help from Patrick Leung.

The research was partially sponsored by the United States Air Force Research Laboratory and the United States Air Force Artificial Intelligence Accelerator and was accomplished under Cooperative Agreement Number FA8750-19-2-1000. The views and conclusions contained in this document are those of the authors and should not be interpreted as representing the official policies, either expressed or implied, of the United States Air Force or the U.S. Government. The U.S. Government is authorized to reproduce and distribute reprints for Government purposes notwithstanding any copyright notation herein.

REFERENCES

- [1] IPCC, "Global warming of 1.5c. an ipcc special report on the impacts of global warming of 1.5c above pre-industrial levels and related global greenhouse gas emission pathways, in the context of strengthening the global response to the threat of climate change, sustainable development, and efforts to eradicate poverty;" 2018. 1, 6
- [2] Centre for Research on the Epidemiology of Disasters (CRED) and UN Office for Disaster Risk Reduction UNISDR, "The human cost of weather-related disasters 1995-2015;" 2015. 1
- [3] NOAA National Centers for Environmental Information (NCEI), "U.S. Billion-Dollar Weather and Climate Disasters (2020)," 2020. [Online]. Available: <https://www.ncdc.noaa.gov/billions/> 1
- [4] S. R. Sheppard, *Visualizing Climate Change A Guide to Visual Communication of Climate Change and Developing Local Solutions*. Taylor and Francis Group, March 2012. 1, 2, 3, 6, 7
- [5] NOAA National Weather Service National Hurricane Center Storm Surge Prediction Unit, "National Storm Surge Hazard Maps, Texas to Maine, Category 5," 2020. [Online]. Available: <https://noaa.maps.arcgis.com/apps/MapSeries/index.html?appid=d9ed7904dbec441a9c4dd7b277935fad&entry=1> 1, 2, 3, 4
- [6] B. Strauss, "Surging seas: Sea level rise analysis," 2015. [Online]. Available: <https://sealevel.climatecentral.org/> 1, 2, 3
- [7] S. R. Sheppard, "Landscape visualisation and climate change: the potential for influencing perceptions and behaviour," *Environmental Science and Policy*, vol. 8, no. 6, pp. 637–654, 2005, mitigation and Adaptation Strategies for Climate Change. 1, 2
- [8] First Street Foundation, "First street foundation flood model technical methodology document," 2020. 2, 3
- [9] Climate Central, "Sea level rise, predicted sea level rise impacts on major cities from global warming up to 4c," 2018. [Online]. Available: https://earthtime.org/stories/sea_level_rise 2, 3, 4

- [10] V. Schmidt, A. Luccioni, S. K. Mukkavilli, N. Balasooriya, K. Sankaran, J. Chayes, and Y. Bengio, “Visualizing the consequences of climate change using cycle-consistent adversarial networks,” *International Conference on Learning Representations (ICLR) Workshop on Tackling Climate Change with AI*, 2019. 1, 2
- [11] R. Gupta, B. Goodman, N. Patel, R. Hosfelt, S. Sajeev, E. Heim, J. Doshi, K. Lucas, H. Choset, and M. Gaston, “Creating xBD: A Dataset for Assessing Building Damage from Satellite Imagery,” in *Proceedings of the IEEE/CVF Conference on Computer Vision and Pattern Recognition (CVPR) Workshops*, June 2019. 2, 3, 9
- [12] P. Isola, J.-Y. Zhu, T. Zhou, and A. A. Efros, “Image-to-image translation with conditional adversarial networks,” in *Computer Vision and Pattern Recognition (CVPR), 2017 IEEE Conference on*, 2017. 1, 2, 5
- [13] T.-C. Wang, M.-Y. Liu, J.-Y. Zhu, A. Tao, J. Kautz, and B. Catanzaro, “High-resolution image synthesis and semantic manipulation with conditional gans,” in *Proceedings of the IEEE conference on computer vision and pattern recognition (CVPR)*, 2018, pp. 8798–8807. [Online]. Available: <https://github.com/NVIDIA/pix2pixHD> 1, 2, 3, 4, 6, 10
- [14] J.-Y. Zhu, T. Park, P. Isola, and A. A. Efros, “Unpaired image-to-image translation using cycle-consistent adversarial networks,” in *Proceedings of the IEEE International Conference on Computer Vision (ICCV)*, Oct 2017. 1
- [15] A. Brock, J. Donahue, and K. Simonyan, “Large scale gan training for high fidelity natural image synthesis,” *arXiv preprint arXiv:1809.11096*, 2018. 1
- [16] C. Requeena-Mesa, M. Reichstein, M. Mahecha, B. Kraft, and J. Denzler, “Predicting landscapes from environmental conditions using generative networks,” in *German Conference on Pattern Recognition*. Springer, 2019, pp. 203–217. 1
- [17] A. Frühstück, I. Alhashim, and P. Wonka, “Tilegan: Synthesis of large-scale non-homogeneous textures,” *ACM Trans. Graph.*, vol. 38, no. 4, Jul. 2019. 1
- [18] T. Mohandoss, A. Kulkarni, D. Northrup, E. Mwebaze, and H. Alemohammad, “Generating synthetic multispectral satellite imagery from sentinel-2,” *NeurIPS 2020 Workshop on AI for Earth Sciences*, 2020. 1
- [19] P. Singh and N. Komodakis, “Cloud-gan: Cloud removal for sentinel-2 imagery using a cyclic consistent generative adversarial networks,” in *IGARSS 2018 - 2018 IEEE International Geoscience and Remote Sensing Symposium*, 2018, pp. 1772–1775. 1
- [20] N. Audebert, B. Le Saux, and S. Lefevre, “Generative adversarial networks for realistic synthesis of hyperspectral samples,” in *IGARSS 2018 - 2018 IEEE International Geoscience and Remote Sensing Symposium*, 2018, pp. 4359–4362. 1
- [21] A. Barredo Arrieta, N. Díaz-Rodríguez, J. Del Ser, A. Bennetot, S. Tabik, A. Barbado, S. Garcia, S. Gil-Lopez, D. Molina, R. Benjamins, R. Chatila, and F. Herrera, “Explainable artificial intelligence (XAI): Concepts, taxonomies, opportunities and challenges toward responsible ai,” *Information Fusion*, vol. 58, pp. 82 – 115, 2020. 1, 6
- [22] D. Bau, J.-Y. Zhu, H. Strobelt, A. Lapedriza, B. Zhou, and A. Torralba, “Understanding the role of individual units in a deep neural network,” *Proceedings of the National Academy of Sciences*, 2020. 1, 2
- [23] A. Madry, A. Makelov, L. Schmidt, D. Tsipras, and A. Vladu, “Towards deep learning models resistant to adversarial attacks,” in *International Conference on Learning Representations (ICLR)*, 2018. 1
- [24] S. Santamaria, D. Dao, B. Lütjens, and C. Zhang, “Truebranch: Metric learning-based verification of forest conservation projects,” *2020 ICLR Workshop on Tackling Climate Change with AI*, 2020. 1
- [25] A. E. R. Tilmann Gneiting, “Weather forecasting with ensemble methods,” *Science*, vol. 310, pp. 248–249, 2005. 1
- [26] A. Lugmayr, M. Danelljan, L. Van Gool, and R. Timofte, “SrfLOW: Learning the super-resolution space with normalizing flow,” in *ECCV*, 2020. 1, 2
- [27] M. Raissi, “Deep hidden physics models: Deep learning of nonlinear partial differential equations,” *Journal of Machine Learning Research*, vol. 19, no. 25, pp. 1–24, 2018. 1, 2
- [28] S. L. Brunton and J. N. Kutz, *Data-Driven Science and Engineering: Machine Learning, Dynamical Systems, and Control*, 1st ed. USA: Cambridge University Press, 2019. 1, 2, 3
- [29] S. Rasp, M. S. Pritchard, and P. Gentine, “Deep learning to represent subgrid processes in climate models,” *Proceedings of the National Academy of Sciences*, vol. 115, no. 39, pp. 9684–9689, 2018. 1
- [30] B. Lütjens, M. Veillette, and D. Newman, “Uncertainty-aware physics-informed neural networks for parametrizations in ocean modeling,” *2020 American Geophysical Union (AGU) Fall Meeting, Session on AI in Weather and Climate Modelling*, 2020. 1
- [31] M. Reichstein, G. Camps-Valls, B. Stevens, M. Jung, J. Denzler, N. Carvalhais, and Prabhat, “Deep learning and process understanding for data-driven earth system science,” *Nature*, vol. 566, pp. 195 – 204, 2019. 2
- [32] M. Raissi, P. Perdikaris, and G. E. Karniadakis, “Physics-informed neural networks: A deep learning framework for solving forward and inverse problems involving nonlinear partial differential equations,” *Journal of Computational Physics*, vol. 378, pp. 686–707, 2019. 2
- [33] B. Lusch, J. Kutz, and S. Brunton, “Deep learning for universal linear embeddings of nonlinear dynamics,” *Nat. Commun.*, vol. 9, 2018. 2
- [34] S. Greydanus, M. Dzamba, and J. Yosinski, “Hamiltonian neural networks,” in *Advances in Neural Information Processing Systems*, vol. 32. Curran Associates, Inc., 2019. 2
- [35] A. T. Mohan, N. Lubbers, D. Livescu, and M. Chertkov, “Embedding hard physical constraints in neural network coarse-graining of 3d turbulence,” *ICLR Workshop on AI for Earth Sciences*, 2020. 2
- [36] T. Lesort, M. Seurin, X. Li, N. Díaz-Rodríguez, and D. Filliat, “Deep unsupervised state representation learning with robotic priors: a robustness analysis,” in *2019 International Joint Conference on Neural Networks (IJCNN)*. IEEE, 2019, pp. 1–8. 2
- [37] C. Rackauckas, Y. Ma, J. Martensen, C. Warner, K. Zubov, R. Supekar, D. Skinner, and A. Ramadhan, “Universal differential equations for scientific machine learning,” *ArXiv*, vol. abs/2001.04385, 2020. 2
- [38] L. A. Garcia and A. Shigidi, “Using neural networks for parameter estimation in ground water,” *Journal of Hydrology*, vol. 318, no. 1, pp. 215–231, 2006. 2
- [39] T. Q. Chen, Y. Rubanova, J. Bettencourt, and D. K. Duvenaud, “Neural ordinary differential equations,” in *Advances in Neural Information Processing Systems 31*. Curran Associates, Inc., 2018, pp. 6571–6583. 2
- [40] A. Karpatne, W. Watkins, J. Read, and V. Kumar, “Physics-guided Neural Networks (PGNN): An Application in Lake Temperature Modeling,” *arXiv e-prints*, p. arXiv:1710.11431, Oct. 2017. 2
- [41] J. Yuval, P. A. O’Gorman, and C. N. Hill, “Use of neural networks for stable, accurate and physically consistent parameterization of subgrid atmospheric processes with good performance at reduced precision,” *Geophysical Research Letter*, vol. 48, p. e2020GL091363, 2021. 2
- [42] Z. Long, Y. Lu, and B. Dong, “PDE-Net 2.0: learning pdes from data with a numeric-symbolic hybrid deep network,” *Journal of Computational Physics*, vol. 399, p. 108925, 2019. 2
- [43] A. Radford, L. Metz, and S. Chintala, “Unsupervised representation learning with deep convolutional generative adversarial networks,” 2016. 2
- [44] C. Wang, H. Zheng, Z. Yu, Z. Zheng, Z. Gu, and B. Zheng, “Discriminative region proposal adversarial networks for high-quality image-to-image translation,” in *Proceedings of the European Conference on Computer Vision (ECCV)*, September 2018. 2
- [45] T. Park, M.-Y. Liu, T.-C. Wang, and J.-Y. Zhu, “Semantic image synthesis with spatially-adaptive normalization,” in *Proceedings of the IEEE Conference on Computer Vision and Pattern Recognition*, 2019. 2
- [46] E. Schönfeld, V. Sushko, D. Zhang, J. Gall, B. Schiele, and A. Khoreva, “You only need adversarial supervision for semantic image synthesis,” in *International Conference on Learning Representations*, 2021. 2, 6
- [47] D. Rezende and S. Mohamed, “Variational inference with normalizing flows,” in *Proceedings of the 32nd International Conference on Machine Learning (ICML)*, F. Bach and D. Blei, Eds., vol. 37, 2015, pp. 1530–1538. 2
- [48] D. P. Kingma and M. Welling, “Auto-encoding variational bayes,” *Proceedings of the 2nd International Conference on Learning Representations (ICLR)*, 2014. 2
- [49] F. P. Casale, A. Dalca, L. Saglietti, J. Listgarten, and N. Fusi, “Gaussian process prior variational autoencoders,” in *Advances in Neural Information Processing Systems*, 2018, pp. 10369–10380. 2
- [50] A. Dosovitskiy and T. Brox, “Generating images with perceptual similarity metrics based on deep networks,” in *Advances in Neural Information Processing Systems 29*. Curran Associates, Inc., 2016, pp. 658–666. 2
- [51] J.-Y. Zhu, R. Zhang, D. Pathak, T. Darrell, A. A. Efros, O. Wang, and E. Shechtman, “Toward multimodal image-to-image translation,” in *Advances in Neural Information Processing Systems (NeurIPS) 30*, 2017, pp. 465–476. [Online]. Available: <https://github.com/junyanz/BicycleGAN> 2, 4
- [52] D. Bau, H. Strobelt, W. Peebles, J. Wulff, B. Zhou, J.-Y. Zhu, and A. Torralba, “Semantic photo manipulation with a generative image prior,” *ACM Trans. Graph.*, vol. 38, no. 4, Jul. 2019. 2
- [53] L. D. Grasso, M. Sengupta, J. F. Dostalek, R. Brummer, and M. Demaria, “Synthetic satellite imagery for current and future environmental satellites,” *International Journal of Remote Sensing*, vol. 29, no. 15, pp. 4373–4384, 2008. 2

- [54] S. J. Cohen, S. Sheppard, A. Shaw, D. Flanders, S. Burch, B. Taylor, D. Hutchinson, A. Cannon, S. Hamilton, B. Burton, and J. Carmichael, "Downscaling and visioning of mountain snow packs and other climate change implications in North Vancouver, British Columbia," *Mitigation and Adaptation Strategies for Global Change planning, Visualization, Water management*, vol. 17, no. 1, pp. 25–49, jan 2012. **2**
- [55] NOAA, "Noaa sea level rise viewer," 2020. [Online]. Available: <https://coast.noaa.gov/slr/> **3, 4**
- [56] C. P. Jelesnianski, J. Chen, and W. A. Shaffer, "Slosh: Sea, lake, and overland surges from hurricanes," *NOAA Technical Report NWS 48, National Oceanic and Atmospheric Administration, U. S. Department of Commerce*, p. 71, 1992, (Scanning courtesy of NOAA's NOS's Coastal Service's Center). **3**
- [57] R. A. Luettich, J. J. Westerink, and N. Scheffner, "ADCIRC: an advanced three-dimensional circulation model for shelves coasts and estuaries, report 1: theory and methodology of ADCIRC-2DDI and ADCIRC-3DL," in *Dredging Research Program Technical Report. DRP-92-6*, U.S. Army Engineers Waterways Experiment Station, 1992, p. 137. **3**
- [58] T.-C. Wang, M.-Y. Liu, J.-Y. Zhu, A. Tao, J. Kautz, and B. Catanzaro, "High-resolution image synthesis and semantic manipulation with conditional gans," in *Proceedings of the IEEE Conference on Computer Vision and Pattern Recognition*, 2018. **3**
- [59] Q. Xu, G. Huang, Y. Yuan, C. Guo, Y. Sun, F. Wu, and K. Weinberger, "An empirical study on evaluation metrics of generative adversarial networks," *arXiv preprint arXiv:1806.07755*, 2018. **3**
- [60] A. Borji, "Pros and cons of gan evaluation measures," *Computer Vision and Image Understanding*, vol. 179, pp. 41–65, 2019. **3, 4**
- [61] D. Ravi, A. B. Szczotka, S. P. Pereira, and T. Vercauteren, "Adversarial training with cycle consistency for unsupervised super-resolution in endomicroscopy," *Medical image analysis*, vol. 53, pp. 123–131, 2019. **4**
- [62] Z. Wang, A. C. Bovik, H. R. Sheikh, and E. P. Simoncelli, "Image quality assessment: from error visibility to structural similarity," *IEEE transactions on image processing*, vol. 13, no. 4, pp. 600–612, 2004. **4**
- [63] W. Bounliphone, E. Belilovsky, M. B. Blaschko, I. Antonoglou, and A. Gretton, "A test of relative similarity for model selection in generative models," 2016. **4**
- [64] T. Salimans, I. Goodfellow, W. Zaremba, V. Cheung, A. Radford, and X. Chen, "Improved techniques for training gans," in *Advances in neural information processing systems*, 2016, pp. 2234–2242. **4**
- [65] C. Tong, L. Yanran, P. J. Athul, B. Yoshua, and L. Wenjie, "Mode regularized generative adversarial networks," in *International Conference on Learning Representations*, 2017. **4**
- [66] M. Heusel, H. Ramsauer, T. Unterthiner, B. Nessler, and S. Hochreiter, "Gans trained by a two time-scale update rule converge to a local nash equilibrium," in *Advances in neural information processing systems*, 2017, pp. 6626–6637. **4**
- [67] S. Zhou, A. Luccioni, G. Cosne, M. S. Bernstein, and Y. Bengio, "Establishing an evaluation metric to quantify climate change image realism," *Machine Learning: Science and Technology*, vol. 1, no. 2, p. 025005, apr 2020. **4**
- [68] R. Zhang, P. Isola, A. A. Efros, E. Shechtman, and O. Wang, "The unreasonable effectiveness of deep features as a perceptual metric," in *CVPR*, 2018. **4**
- [69] USDA-FSA-APFO Aerial Photography Field Office, "National Geospatial Data Asset National Agriculture Imagery Program (NAIP) Imagery," 2019. [Online]. Available: <http://gis.apfo.usda.gov/arcgis/rest/services/NAIP> **5**
- [70] Maxar DigitalGlobe, "Open data program, hurricane harvey, 8/31/2017, tileid: 105001000b95e100." [Online]. Available: <https://www.maxar.com/open-data/> **5**
- [71] E. F. Thomas, C. McGarty, and K. I. Mavor, "Transforming "apathy into movement": the role of prosocial emotions in motivating action for social change," *Personality and Social Psychology Review*, vol. 13, no. 4, pp. 310–333, 2009. **5**
- [72] P. Slovic, M. L. Finucane, E. Peters, and D. G. MacGregor, "Risk as analysis and risk as feelings: Some thoughts about affect, reason, risk, and rationality," *Risk Analysis*, vol. 24, no. 2, pp. 311–322, 2004. **5**
- [73] S. Bamberg and G. Möser, "Twenty years after hines, hungerford, and tomara: A new meta-analysis of psycho-social determinants of pro-environmental behaviour," *Journal of Environmental Psychology*, vol. 27, no. 1, pp. 14–25, 2007. **5**
- [74] S. O'Neill and S. Nicholson-Cole, "'fear won't do it': Promoting positive engagement with climate change through visual and iconic representations," *Science Communication*, vol. 30, no. 3, pp. 355–379, 2009. **5**
- [75] M. Ojala, "Hope and climate change: the importance of hope for environmental engagement among young people," *Environmental Education Research*, vol. 18, no. 5, pp. 625–642, 2012. **5**
- [76] NASA/Goddard Space Flight Center Scientific Visualization Studio, "Annual arctic sea ice minimum 1979-2020 with area graph," 2020, last accessed March 2021. [Online]. Available: https://climate.nasa.gov/climate_resources/155/video-annual-arctic-sea-ice-minimum-1979-2020-with-area-graph/ **6**
- [77] A. Lacoste, E. D. Sherwin, H. Kerner, H. Alemohammad, B. Lütjens, J. Irvin, D. Dao, A. Chang, M. Gunturkun, A. Drouin, P. Rodríguez, and D. Vázquez, "Toward foundation models for earth monitoring: Proposal for a climate change benchmark," *CoRR*, vol. abs/2112.00570, 2021. **6**
- [78] M. C. Hansen, P. V. Potapov, R. Moore, M. Hancher, S. A. Turubanova, A. Tyukavina, D. Thau, S. V. Stehman, S. J. Goetz, T. R. Loveland, A. Kommareddy, A. Egorov, L. Chini, C. O. Justice, and J. R. G. Townshend, "High-resolution global maps of 21st-century forest cover change," *Science*, vol. 342, no. 6160, pp. 850–853, 2013. **6**
- [79] K. Anderson, B. Ryan, W. Sonntag, A. Kavvada, and L. Friedl, "Earth observation in service of the 2030 agenda for sustainable development," *Geo-spatial Information Science*, vol. 20, no. 2, pp. 77–96, 2017. **6**
- [80] X. Zhu, D. Tuija, L. Mou, G.-S. Xia, L. Zhang, F. Xu, and F. Fraundorfer, "Deep learning in remote sensing: A comprehensive review and list of resources," *IEEE Geoscience and Remote Sensing Magazine*, vol. 5, pp. 8–36, 12 2017. **7**
- [81] M. S. Veillette, E. P. Hassey, C. J. Mattioli, H. Iskenderian, and P. M. Lamey, "Creating synthetic radar imagery using convolutional neural networks," *Journal of Atmospheric and Oceanic Technology*, vol. 35, no. 12, pp. 2323–2338, 2018. **7**
- [82] G. Di Baldassarre, G. Schumann, and P. Bates, "Near real time satellite imagery to support and verify timely flood modelling," *Hydrological Processes*, vol. 23, no. 5, pp. 799–803, 2009. **7**
- [83] DigitalGlobe, "Open data for disaster response," 2020. [Online]. Available: <https://www.digitalglobe.com/ecosystem/open-data> **9**
- [84] P. Y. Simard, D. Steinkraus, J. C. Platt *et al.*, "Best practices for convolutional neural networks applied to visual document analysis." in *Icdar*, vol. 3, no. 2003, 2003. **10**
- [85] T. Miyato, T. Kataoka, M. Koyama, and Y. Yoshida, "Spectral normalization for generative adversarial networks," *2018 International Conference on Learning Representations (ICLR)*, 2018. **10**
- [86] A. Buslaev, A. Parinov, E. Khvadchenya, V. I. Iglovikov, and A. A. Kalinin, "Albumentations: fast and flexible image augmentations," *arXiv e-prints*, 2018. **10**
- [87] C. Robinson, L. Hou, K. Malkin, R. Soobitsky, J. Czawlytko, B. Dilkina, and N. Jovic, "Large scale high-resolution land cover mapping with multi-resolution data," in *Proceedings of the IEEE Conference on Computer Vision and Pattern Recognition (CVPR)*, 2019. **11**

APPENDIX A DATASET

A. Pre- and post-flood imagery

Post-flood images that display standing water are challenging to acquire due to cloud-cover, time of standing flood, satellite revisit rate, and cost of high-resolution imagery. To the extent of the authors' knowledge, xBD [11] is the best publicly available data-source for preprocessed high-resolution imagery of pre- and post-flood images. More open-source, high-resolution, pre- and post-disaster images can be found in unprocessed format on DigitalGlobe's Open Data repository [83].

- Data Overview: 3284 flood-related RGB image pairs from seven flood events at 1024×1024 px of ~ 0.5 m/px resolution of which 30% display a standing flood (~ 1370).
- The dataset contains imagery of hurricanes (Harvey, Florence, Michael, Matthew in the U.S. East or Gulf Coast), spring floods (2019 in Midwest U.S.), a tsunami (in Indonesia), and the monsoon (in Nepal).
- Our evaluation test set is composed of 216 images: 108 images of each hurricane Harvey and Florence. The test

set excludes imagery from hurricane Michael or Matthew, because the majority of tiles does not display standing flood.

- We did not use digital elevation maps (DEMs), because the information of low-resolution DEMs is contained in the storm surge model and high-resolution DEMs for the full U.S. East Coast were not publicly available.

B. Pre- and post-forestation imagery

We went through all of VERA [source] registered ARR (Afforestation, Reforestation, and Revegetation) carbon projects, and downloaded the shapefiles (.kmz) when they were available. We used Google Earth Pro [source] to first confirm that historical imagery was available, meaning that high-resolution imagery was available over the years for the specific regions from the shapefiles and had no clouds. Then we visually verified that the reforestation did happen. These conditions were considered satisfied if we had imagery of bare land where we could see trees planted and grown over the years. In that case, we considered “pre-forestation” as the earliest available imagery before we could see that trees were planted. For instance, if on the high-resolution imagery, we saw that trees were planted in 2010, then we would go back in time to the previously available imagery which could be 2009 or 2005, depending on the regions. For the “post-forestation” imagery, we selected the most recent imagery available without clouds, so ideally it would be 2022. Our dataset timestamps go from 2005 to 2022 with some in-between years when those years were not available or not good quality (too many clouds, overlapping rasters from different years, etc).

Ultimately, the selected high-resolution images of before and after reforestation were exported from Google Earth Pro (Map data: Google, Maxar Technologies, CNS/Airbus) with a resolution of 4800x4800 and an eye altitude of 1500 meters. The image of the pre-forestation with the visual of the shapefile layer was also exported to be then used as the binary reforested area mask. The image with the visual of the shapefile was converted to a binary mask using an image processing method that removed all non-white pixels.

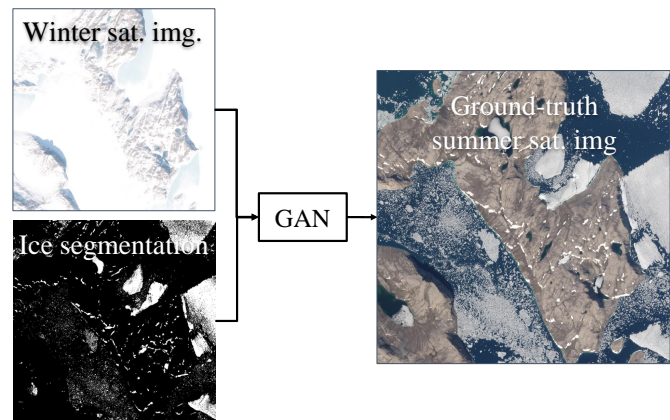
The 1024x1024 tiles were generated from the 4800x4800 exported images. The binary reforestation area masks were stacked on top of the RGB images. Only tiles that had pixels belonging to a reforested area were saved.

C. Pre- and post-melt Arctic sea ice imagery

To visualize melting Arctic sea ice we created 19445 image-triplets of pre-melt image, post-melt image, and post-melt segmentation mask, as displayed in Fig. 9. We found $\sim 20k$ matching pre- and post-melt images by finding matching pairs across 27172 Winter images in 1st Oct. 2019 - 1st May 2020 and 32433 Summer images in 1st Jun. - 31st Aug. 2020 within the study area in Fig. 10a. We downloaded cloud-free Sentinel-2 MSI Level 1-C visual imagery at 10m/px resolution in tiles of 1024x1024px that matched the criteria. Our ice segmentation model creates binary ice segmentation masks (1=ice) by thresholding grayscale images into white and non-white (intensity ≥ 255) areas, $x = (1 \text{ if } x==1 \text{ else } 0)$.



(a) Data samples



(b) Model architecture

Fig. 9: We allow the extension of *Earth Intelligence Engine* to visualize melting Arctic sea ice by publishing an according dataset.

We created the post-melt segmentation masks by applying the segmentation model on the post-melt imagery. After creating segmentation masks, we rejected all image pairs that only contain ocean or land (mask=0). Figure 10b shows the final locations of all image pairs.

APPENDIX B EXPERIMENTS

A. Data Augmentation.

To visualize floods, we applied standard data augmentation, here rotation, random cropping, hue, and contrast variation, and state-of-the-art augmentation - here elastic transformations [84]. Furthermore, spectral normalization [85] was used to stabilize the training of the discriminator. A relativistic loss function has been implemented to stabilize adversarial training. We also experimented with training pix2pixHD on LPIPS loss. Quantitative evaluation of these experiments, however, showed that they did not have significant impact on the performance and, ultimately, the results in the paper have been generated by the pytorch implementation of pix2pixHD [13] extended to 4-channel inputs.

To visualize reforestation, we used downscale (to 0.8 scale), h- and v-flip, and colorjitter (brightness=0.4, contrast=0.2, saturation=0, hue=0) augmentations with $p = 0.67$ from the albumentations library [86]. The model hyperparameters are chosen to equal the pytorch implementation in [13].

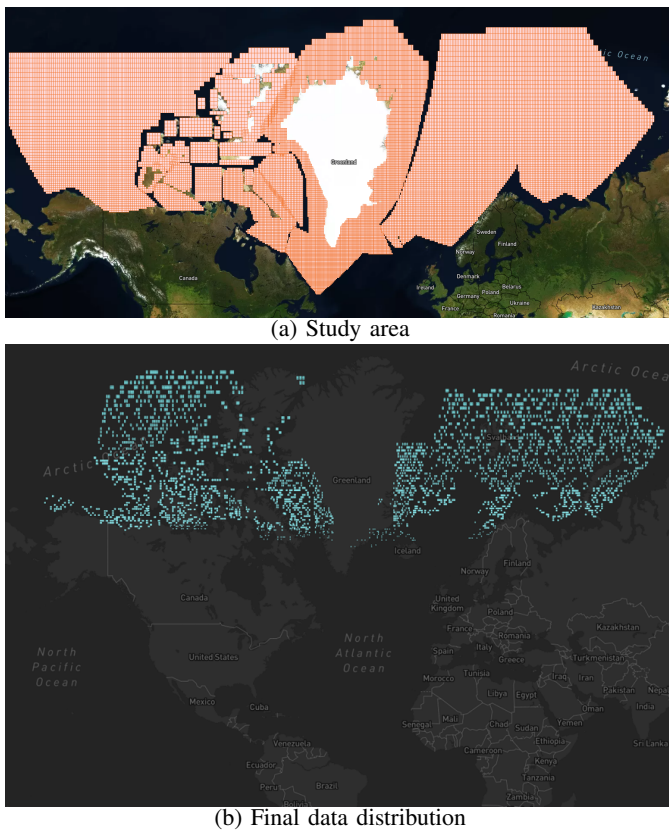


Fig. 10: We compiled a dataset of $\sim 20k$ image-pairs of the Arctic to visualize melting Arctic sea ice.

B. Pre-training LPIPS on satellite imagery.

The standard LPIPS did not clearly distinguish in between the handcrafted baseline and the physics-informed GAN, contrasting the opinion of a human evaluator. This is most likely because LPIPS currently leverages a neural network that was trained on object classification from ImageNet. The neural network might not be capable to extract meaningful high-level features to compare the similarity of satellite images. In preliminary tests the ImageNet-pretrained network would classify all satellite imagery as background image, indicating that the network did not learn features to distinguish satellite images from each other. Future work, will use LPIPS with a network trained to have satellite imagery specific features, e.g., Tile2Vec or a land-use segmentation [87] model.

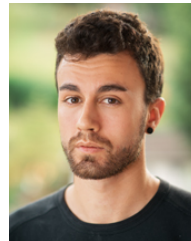


Björn Lütjens is a PhD candidate at the Human Systems Laboratory, Department of Aeronautics and Astronautics, MIT. Together with Prof. Dava Newman, Dr. Cait Crawford, and Prof. Youssef Marzouk, he works on tackling climate change with machine learning. As deep learning algorithms are widely considered "black-box," his work focuses on increasing trust and transparency when using deep learning in monitoring, predicting, and visualizing climate variables. His work includes physics-informed neural networks to quantify the uncertainty in localized climate projections and physically-consistent GANs for visualizing coastal floods. He is also monitoring forest carbon from aerial imagery, which is supported by Microsoft, NASA, WWF, MIT PkG, MIT Legatum, and MIT Sandbox. He has previously obtained his M.Sc at MIT in Autonomous Systems, pioneering with Prof. Jon How safe and robust deep reinforcement learning techniques. More information available at blutjens.github.io.



Brandon Leshchinskiy is a dual SM candidate studying Aeronautics & Astronautics and Technology & Policy at the Massachusetts Institute of Technology. He works with Apollo Professor and former NASA Deputy Administrator Dava Newman, building AI tools to adapt to climate change and educational tools to stop it. Prior to graduate school, Brandon worked as a data scientist at MIT Lincoln Laboratory, where he developed technologies for American security. Brandon holds a B.S. in electrical engineering from Penn State University. Outside of

work, Brandon dances, plays piano, and does improv theater. Or at least, he did before Covid.



Christian Requena-Mesa is a PhD Student in environmental science at the Department Biogeochemical Integration, Max Planck Institute for Biogeochemistry and the German Aerospace Center (DLR). He is interested on how novel computer vision and generative algorithms can improve environmental monitoring, as well as, how artificial general intelligence can lead to a better environmental management and decision making. His vision for environmental problem solving relies on the use of deep learning as a dynamic adviser to help us set the rules by which humans best interact with the environment. He believes that current artificial intelligence can help in finding the equilibrium that maximizes both: the benefits we get from nature, and the stability and resilience of the natural systems.



Farrukh Chishtie is an atmospheric and Earth observation scientist with extensive experience in various experimental and modelling disciplines. He has more than seventeen years of research experience, which includes work with the USAID NASA SERVIR-Mekong Program and Cloud Physics and Severe Weather Research Section, Environment and Climate Change Canada (ECCC). He was part of the Canadian CloudSat CALIPSO Validation (C3VP) project. He holds doctoral degrees in both Natural and Social Sciences from the University of Western

Ontario, Canada with undergraduate and graduate degrees in engineering and applied mathematics from the USA. Presently, he holds visiting scientist and faculty positions at ECCC, CERN Theory Group, University of Toronto and University of Western Ontario.



Natalia Díaz-Rodríguez is Assistant Prof. of Artificial Intelligence at the Autonomous Systems and Robotics Lab (U2IS) at ENSTA Paris, Institut Polytechnique Paris. She also belongs to the INRIA Flowers team on developmental robotics. Her research interests include deep, reinforcement and unsupervised learning, (state) representation learning, explainable AI and AI for social good. She is working on open-ended learning and continual/lifelong learning for applications in computer vision and robotics. Her background is on knowledge engineering (semantic web, ontologies and knowledge graphs) and is interested in neural-symbolic approaches to practical applications of AI.



Océane Boulais is a Research Engineer at the National Oceanic and Atmospheric Agency and Northern Gulf Institute leading the development of real-time classification and detection algorithms for in-situ habitat cameras to quantify reef fish species and bycatch heuristics from electronic monitoring systems aboard shrimp trawlers in the Gulf of Mexico. She holds a Master's degree from MIT Media Lab's Responsive Environment group in she was involved in fieldwork with National Geographic's Exploration Technology Lab deploying drop cameras to perform benthic floor mapping in the Galapagos and collaborations with NGO Conservation International to design and deploy a computer vision system for marine resource management aboard Pacific Island tuna fishery vessels.



Aruna Sankaranarayanan is a Master's student at the MIT Media Lab's Viral Communications group and works with Prof. Andrew Lippman. She is interested in misinformation, Earth observation, and climate change. Prior to joining MIT, she has contributed to open-source work at the Humanitarian OpenStreetMap Team, worked as an infrastructure engineer at Mapbox, and contributed to the GCompris Project. She worked with Dr. Abhishek Nagaraj at University of California Berkeley on analyzing the contributing community of OpenStreetMap. She holds a B.Sc. in Computer Science from the BMS Institute of Technology and Management. Apart from work, Aruna is an avid writer and interested in outreach activities.



Margaux Masson-Forsythe is a Science Machine Learning engineer at Earthshot Labs where she works on developing spatially explicit models for risk assessment, computer vision models for automatic tree measurements, and generative adversarial networks for visual simulation of reforestation. Her research interests include machine learning, deep learning, computer vision, software engineering, product development, image processing, and the broader application of AI for climate-related issues. She has worked on several projects using deep learning for climate issues, such as deforestation detection in the Congo Basin, crop yield prediction in Senegal, and classification of facility rooftops to determine solar installation potential. She is also a science writer and a strong advocate for diversity in STEM.



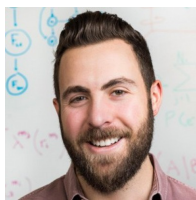
Aaron Piña is a AAAS Science and Technology Policy Fellow at NASA Headquarters. He works as a Deputy Program Scientist in the Science Mission Directorate, Earth Science Division to support the Weather and Atmospheric Dynamics Focus Area in weather research, data, and technology. Prior to joining NASA Headquarters, Aaron worked as a scientist for Aeris, LLC. Aaron earned his B.S. degree in Meteorology from Texas A&M University, his M.S. in Atmospheric Science from Colorado State University, and his Ph.D. in Ecology from Colorado State University. He is a member of the American Meteorological Society, the American Geophysical Union, and the American Association for the Advancement of Science.



Yarin Gal leads the Oxford Applied and Theoretical Machine Learning group (OATML) at the University of Oxford. He is the Associate Professor of Machine Learning at the Computer Science department, and is also the Tutorial Fellow in Computer Science at Christ Church, Oxford, and an AI Fellow at the Alan Turing Institute, the UK's national institute for artificial intelligence. Prior to his move to Oxford he was a Research Fellow in Computer Science at St Catharine's College at the University of Cambridge. He obtained his PhD from the Cambridge machine learning group, working with Zoubin Ghahramani FRS and funded by the Google Europe Doctoral Fellowship. Yarin made substantial contributions to early work in modern Bayesian deep learning quantifying uncertainty in deep learning and developed ML/AI tools that can inform their users when the tools are "guessing at random". These tools have been deployed widely in industry and academia, with the tools used in medical applications, robotics, computer vision, astronomy, in the sciences, and by NASA.



Chedy Raïssi received his PhD in Computer Science from the Ecole des Mines d'Alès in July 2008. After completing his PhD, Chedy worked as a research fellow (post-doctoral researcher) at the National University of Singapore on privacy-preserving data mining with emphasis on the anonymization of clinical trial data. In 2010, Chedy was appointed as a permanent research scientist (chargé de recherche) at the French Institute for Research in Computer Science and Automation (INRIA), France where he joined the Orpailleur team and worked in the field of sequence and graph combinatorics and concept lattices (also known as "Galois lattices"). Since 2019, Chedy is on a sabbatical leave from INRIA and joined Ubisoft Singapore as the Data Science Director where he leads a new team of researchers and engineers to shape up innovative projects for machine learning and video games.



Alexander Lavin spent much of his career at the intersection of AI and neuroscience. He founded Latent Sciences to develop a patented AI platform (i.e. a probabilistic programming domain-specific language he built) for predictive and causal modeling neurodegenerative diseases, which was acquired into a stealth enterprise AI company. Prior to Latent Sciences, he worked with Vicarious and Numenta towards artificial general intelligence. Prior to pursuing AI, he was a spacecraft engineer, working with NASA, Blue Origin, Astrobotic, and Technion. He

is a technical lead with nasa.ai for various ML projects in climate science and astronaut health, and leading novel initiatives in Systems ML and a Forbes 30 Under 30 honoree in Science. He studied computational mechanics and robotics at Carnegie Mellon (under advisors Red Whittaker and Kenji Shamada), engineering management at Duke University, and mechanical and aerospace engineering at Cornell. Away from the computer he is a runner, yogi, outdoors explorer, and dog dad. More information available at lavin.io.



Dava Newman is the Apollo Program Professor of Astronautics and Director of the MIT-Portugal Program at the Massachusetts Institute of Technology, and a Harvard-MIT Health, Sciences, and Technology faculty. Her aerospace biomedical engineering research investigates human performance across the spectrum of gravity, including space suits, life support and astronaut performance. She has been the PI on 4 spaceflight missions. Her second skin Bio-Suit™ planetary spacesuit inventions are now being applied to soft exoskeletons to enhance locomotion

on Earth. She has exhibited the BioSuit™ at the Venice Biennial, London's Victoria and Albert Museum, Paris' Cite des Sciences et de L'Industrie, American Museum of Natural History, and Metropolitan Museum of Art. Her current research targets climate change and Earth's vital signs from Oceans-to-Space. She has circumnavigated, sailing around the world. She is the PI on the Earth Intelligence Engine AI platform for weather and climate. Newman is the author of the text Interactive Aerospace Engineering and Design and has over 300 publications. Dr. Newman served as NASA Deputy Administrator from 2015–2017, and was responsible for articulating NASA's vision, providing leadership and policy direction, spear-heading diversity and inclusion, and representing NASA to the White House, Congress, international space agencies, and industry. Dr. Newman was the first female engineer and scientist to serve in this role and was awarded the NASA Distinguished Service Medal.